Fibrillarin-1 and Fibrillarin-2 are required for divergent cell lineage development in planarian homeostasis and regeneration

Jiajia Chen[1,2,3], Xue Pan[1,2,3], Hao Xu[1,2,3], Yuhong Zhang[2,3], Kai Lei[2,3,*]

1. School of Life Sciences, Zhejiang University, Hangzhou, Zhejiang, China
2. Westlake Laboratory of Life Sciences and Biomedicine, Key Laboratory of Growth Regulation and Translational Research of Zhejiang Province, School of Life Sciences, Westlake University, Hangzhou, Zhejiang, China
3. Institute of Biology, Westlake Institute for Advanced Study, Hangzhou, Zhejiang, China

*To whom correspondence should be addressed. E-mail: leikai@westlake.edu.cn (K.L.)

Keywords: planarian, ribosome, rRNA modification, epidermal lineage, cell differentiation

Abstract

Ribosome heterogeneity has been revealed to exist in different cell types during development. However, the function and regulatory mechanisms of ribosome heterogeneity in missing tissue regeneration have yet to be reported. We used the planarian *Schmidtea mediterranea* with whole-body regenerative capability as a model and revealed the function of the rRNA modification protein fibrillarin in cell lineage development and tissue regeneration. We identified two fibrillarin homologs in planarian, *Smed-fbl-1* (*fbl-1*) and *Smed-fbl-2* (*fbl-2*), with distinct expression patterns. While *fbl-2* regulates stem cell proliferation and multiple progenitor cell differentiation, *fbl-1* participates in epidermal lineage late-stage specification and wound response. This study indicates that fibrillarin, a nucleolar protein, can respond to wounds and function in distinct cell types, suggesting the existence and critical roles of ribosome heterogeneity in stem cells and tissue regeneration.

Introduction

Ribosomal biogenesis is the basis for multiple cellular processes, and its dysfunction influences translation, cell cycle, and immune responses (Bianco & Mohr, 2019; Kang *et al*, 2021; Pelletier *et al*, 2018; Xu *et al*, 2016). Ribosomes are composed of two major components, the large and small ribosomal subunits (LSU and SSU). Each subunit consists of specific ribosomal RNA (rRNA; LSU: 28S rRNA, 5.8S rRNA, and 5S rRNA; SSU: 18S rRNA) and ribosomal proteins (RPs; LSU: RPLs; SSU: RPSs). Ribosome heterogeneity was proposed early in 1958 and revised to the ribosome filter hypothesis in 2002 (Gay *et al*, 2022; Genuth & Barna, 2018; Li & Wang, 2020). Ribosome heterogeneity can be determined by rRNA variants and modifications, RPs, and other factors, including ribosome-associated proteins, subcellular localization of ribosomes, and the ribosomal architecture (Li & Wang, 2020). Its origination remains to be addressed, including distinctly heterogeneous ribosome components, cell-type-specific or subcellular-compartment-specific ribosomes, and recognition and production of specific ribosomes (Gay *et al.*, 2022; Genuth & Barna, 2018). rRNA modification is a prominent source of ribosome heterogeneity, with the most abundant type being 2'-O-methylation. Different cell types have diverse profiles of 2'-O-methylation, providing evidence of the ribosome heterogeneity (Krogh *et al*, 2016). Numerous studies have also implied that stem cell differentiation and cell fate determination require increasing ribosome biogenesis and protein synthesis in multiple species (Gay *et al.*, 2022; Lv *et al*, 2021; Sanchez *et al*, 2016; Zhang *et al*, 2014). Whether ribosome heterogeneity occurs during stem cell differentiation or cell type specification *in vivo* remains to be explored.

Fibrillarin (FBL) is an essential nucleolar protein that is conserved in organisms ranging from yeast to humans. The main structure of FBL contains two functional domains: a glycine/arginine-rich (GAR) region with nuclear localization signals and an RNA binding domain with methyltransferase (MTase) activity (Pereira-Santana *et al*, 2020; Rodriguez-Corona *et al*, 2015). Depending on its functional domain, FBL catalyzes the 2'-O-methylation of rRNA to process pre-rRNA into 18S rRNA and 28S rRNA. Previous studies have illustrated that FBL functions in the nucleolus to process rRNA through

liquid-liquid phase separation via its GAR domain (Yao *et al*, 2019). Guided by small nucleolar RNA (snoRNA), FBL participates in different cellular processes (Li *et al*, 2018; Ren *et al*, 2019; Yi *et al*, 2021). FBL can regulate stem cell viability and control stem cell differentiation through the p53 signaling pathway (Watanabe-Susaki *et al*, 2014). Inhibition or mutation of FBL influences the mouse early development (Newton *et al*, 2003), arrests cells at the S-phase of the cell cycle and impairs neuron differentiation in zebrafish (Bouffard *et al*, 2018). Considering the role of FBL in stem cell biology, we hypothesized that FBL generates ribosome heterogeneity by rRNA modification to regulate the development of stem cells during tissue homeostasis and regeneration.

Planarian is considered as a remarkable animal model that can be used to investigate regeneration mechanisms. Using planarians, which have the whole-body regenerative capability, allowed us to explore the functions of genes from the perspective of the stem cell biology (Reddien, 2018). Proper neoblast proliferation and differentiation are critical for cell renewal and regeneration after amputation or injury (Scimone *et al*, 2014). The precise regulation of neoblasts self-renew and differentiate to replace missing tissue or maintain homeostasis is still being studied (Bohr *et al*, 2021; Boser *et al*, 2013; Lei *et al*, 2016; Reddien, 2018, 2021; Wagner *et al*, 2012; Wenemoser & Reddien, 2010).

We found two homologs of FBL in planarians. Regenerative capacity was destroyed after the knockdown of *Smed-fbl-1* (*fbl-1*) or *Smed-fbl-2* (*fbl-2*). In line with the function of FBL, the rRNA expression levels were decreased in animals subjected to RNA interference (RNAi). Evidence regarding cell-type-specific ribosomes was obtained via analysis of the cell types differentially expressing *fbl-1* and *fbl-2*. *fbl-1* was explicitly expressed in *AGAT-1*$^{+}$ cells and their mature descendants, whereas *fbl-2* was expressed in progenitor cells and stem cells. Upon dissecting the functions of the two homologs in planarians during homeostasis and regeneration, we propose that *fbl-1* and *fbl-2* differentially regulate cell proliferation, differentiation, and even epidermal cell specification through specific ribosome translation.

Results

Knockdown of *Smed-fbl-1* or *Smed-fbl-2* shows distinct defects in homeostasis

The human FBL sequence was used to search for homologs in the planarian *Schmidtea mediterranea* by protein sequence alignment. Both evolutionary conservation and cellular expression patterns validated the homologs of FBL in planarians. SMED30025294 and SMED30005569, termed *fbl-1* and *fbl-2*, respectively, were predicted to encode FBL after performing a phylogenetic comparison and analyzing the GAR and MTase functional domains (Fig 1A). Distinct from the nucleolar localization of both FBL proteins in H9 cells, FBL-2 is located at the cytoplasm in 293T cells, suggesting the different cellular localization of FBL-2 in various cell types (Fig EV1A and B).

To investigate the functions of these homologs in planarians, we performed RNAi experiments to knock down the expression of *fbl-1* and *fbl-2*, respectively. Both *fbl-1* and *fbl-2* are required for homeostasis, supporting the essential function of FBL at the same feeding schedule (Figs 1B-D, EV1C). Upon observation of the defects, *fbl-1* knockdown (KD) animals showed white spots on the dorsal epidermis before tail breaking and body disassembly (lethal phenotype) (Fig 1C). By contrast, 57% of *fbl-2* KD animals displayed head regression and then disassembly, while others remained intact (Fig 1C). These phenomena suggested that *fbl-1* and *fbl-2* play diverse roles in homeostasis.

***Smed-fbl-1* and *Smed-fbl-2* are required for homeostasis and regeneration by modulating rRNA expression**

To observe the regenerative capacity of *fbl-1* KD animals, we modified the RNAi feeding schedule as shown in Figure 2A. The animals still displayed different effects on homeostasis after KD of *fbl-1* or *fbl-2* (Fig 2B and C). Lesions appeared in the tail of *fbl-1* KD animals, but *fbl-2* KD animals exhibited head regression (Fig 2B and C). These phenotypes led us to explore the functional difference between *fbl-1* and *fbl-2* in planarians. Quantitative real-time PCR (qPCR) was used to confirm the KD efficiency. The results showed that KD of *fbl-1* did not influence the expression of *fbl-2*, and vice versa (Fig 2D and E). Furthermore, the decreased expression of FBL-2

after KD of *fbl-2* was validated by anti-FBL-2 antibody immunofluorescent staining in *fbl-2* KD animals compared with that in *egfp* KD controls (Fig EV1D). To confirm the functions of *fbl-1* and *fbl-2* in rRNA biogenesis, we performed qPCR to measure the relative amounts of 18S rRNA and 28S rRNA in *fbl-1* or *fbl-2* KD planarians, respectively. Both *fbl-1* KD and *fbl-2* KD planarians had significantly lower 18S rRNA and 28S rRNA levels than *egfp* KD controls (Fig 2F-I). Taken together, these results suggested that *fbl-1* and *fbl-2* are conserved to modulate rRNA biogenesis.

To examine the functions of *fbl-1* and *fbl-2* in missing tissue regeneration, we amputated the KD animals seven days after the last feeding. The *fbl-1* KD animals regenerated more slowly and exhibited smaller blastema, while the *fbl-2* KD animals could not regenerate the anterior and posterior tissues (Figs 2J-K, EV2A). The blastema formation involves the expression of wound response genes, proliferation and differentiation of neoblasts, and guidance of the positional signals (Reddien, 2018; Wenemoser *et al*, 2012; Wenemoser & Reddien, 2010). However, a comparison of the levels of early response genes (*fos1*, *jun1*, and *runt1*) showed normal induction of the wound response in *fbl-2* KD animals (Fig EV2B). The staining of various tissues confirmed the regeneration defects after KD of *fbl-1* or *fbl-2*, which showed incompletely regenerative CNS and intestinal branches at 7 days post-amputation (dpa) (Fig 2L). The regeneration defects were further confirmed by the disrupted formation of anterior (*notum*) and posterior (*wnt-1*) polarity in both *fbl-1* KD and *fbl-2* KD animals at 72 hours post-amputation (hpa) (Fig 2M). Unlike *fbl-1* KD animals, the expression of *notum* and *wnt-1* is obviously affected in *fbl-2* KD animals, suggesting the disturbed expression of positional control genes by *fbl-2* KD.

Smed-fbl-1 **and** ***Smed-fbl-2*** **are expressed in distinct cell types**

To examine how *fbl* inhibition causes regeneration and homeostasis defects, whole-mount in situ hybridization (WISH) and fluorescent in situ hybridization (FISH) of planarians were performed to elucidate the expression patterns of *fbl-1* and *fbl-2* (Fig 3A, F). The spatial expression pattern along the DV axis showed that the *fbl-1*$^{+}$ cells were distributed from the dorsal mesenchyme to the dorsal epidermis, but the *fbl-2*$^{+}$

cells were distributed extensively (Fig 3A, F). Based on the above expression patterns, we first proposed that *fbl-1* is expressed in epithelial lineage cells. The development of planarian epithelial cells has been identified with multiple progenitor types through the lineage (Cheng *et al*, 2018; Tu *et al*, 2015; Wurtzel *et al*, 2015; Zhu *et al*, 2015; Zhu & Pearson, 2018). The *prog-1*$^+$ and *AGAT-1*$^+$ cells have been identified as early and late progenitors of the epithelial lineage (Eisenhoffer *et al*, 2008). *AGAT-1*$^+$ cells have been further characterized as specifiers of mature epithelium, while *vim-3*$^+$ cells are produced after the *zpuf-6*$^+$ transient state (Tu *et al.*, 2015). Therefore, through double FISH (dFISH) to co-label *fbl-1*$^+$ cells with epithelial lineage markers, we showed that *fbl-1* is expressed in epithelial lineage cells, distinctly in *AGAT-1*$^+$ cells. The ratio of cells co-expressing *AGAT-1* and *fbl-1* was high (agat-1/fbl-1: 99.5%), whereas smaller proportion of *fbl-1* co-expression was observed in *vim-3*$^+$ or *zpuf-6*$^+$ cells (zpuf-6/fbl-1: 11.6%, vim-3/fbl-1: 31.9%) (Fig 3B). Furthermore, *fbl-1* transcript levels were increased after amputation at the anterior-faced or posterior-faced wound sites during regeneration initiation (4-24 hpa), suggesting a wound response at the level of *fbl-1* transcription (Fig 3C). Notably, the expression of *fbl-1* retained a pattern similar to that in intact worms and was comparable to that in the control group at 48 hpa (Figs 3C, EV3C). At 72 hpa, the knockdown efficiency was restored, and *fbl-1* was highly co-expressed within *vim-3*$^+$ cells (Fig 3D and E). This evidence suggested that ribosome biogenesis and protein synthesis are required during stem cell differentiation, which triggers high expression of *fbl-1* (overload) rather than inhibiting *fbl-1*. In addition, *fbl-1* was not expressed at the blastema at 48 hpa, where *AGAT-1*$^+$ cells will accumulate, suggesting that *fbl-1* is expressed in the late stage of *AGAT-1*$^+$ cells without affecting their generation.

We second predicted that *fbl-2* is expressed in stem cells or progenitor cells based on the evidence that 1) KD of *fbl-2* caused head regression, reflecting a defect in stem cells (Reddien *et al*, 2005); 2) most *fbl-2*$^+$ cells were depleted at one-day post-irradiation (dpi) (Fig 3G). The dFISH experiments showed that *fbl-2* was expressed widely in different cell types. Given that *fbl-1* was expressed in epidermal lineage, we

next examined whether *fbl-2* also facilitated epidermal cell differentiation. The signals of *fbl-2* co-expressed in *prog-1*$^+$ cells were evident, whereas those of *fbl-2* co-expressed in neoblasts were dot-like (Figs 3H, EV3E). Some unknown cell types also expressed *fbl-2* (Fig EV3A and B). In addition, *fbl-2* was stimulated at the wound site at 24 hpa when the stem cells were activated for proliferation and differentiation (Fig 3G). This finding is consistent with the co-expression of *fbl-2* with early progenitor and stem cell markers. In contrast to the expression of *fbl-1* at the early time point after amputation, *fbl-2* did not respond to wounds but was parallel to the waves of H3P expression at 6 and 48 hpa, which is also consistent with the normal expression of wound-induced genes after KD of *fbl-2* (Figs EV2B, EV3D). The above results suggested that FBL-1 functions in epidermal cell lineage development, especially the specification from *AGAT-1*$^+$ cells to *zpuf-6*$^+$ and *vim-3*$^+$ cells, while FBL-2 functions in stem cells and progenitor cells to regulate cell proliferation or differentiation.

Smed-fbl-2 is required for stem cell proliferation and differentiation into early progenitors

To elucidate the cellular mechanisms regulated by *fbl-1* and *fbl-2*, we first examined the stem cell population (*piwi-1*$^+$) and proliferating cell population (H3P$^+$) in *fbl-1* and *fbl-2* KD worms. Compared with *egfp* KD and *fbl-1* KD worms, only *fbl-2* KD planarians exhibited reductions in the number of proliferative cells during homeostasis, consistent with the expression of *fbl-2* in neoblasts and the head regression phenotype (Figs 4A and B, EV5A-D). The *fbl-2* KD animals almost maintained complete but shrank bodies. The number of neoblasts (*piwi-1*+) decreased slightly at seven days post-feeding (dpf) (Fig EV4A). However, the H3P signals were significantly reduced after KD of *fbl-2* during homeostasis and regeneration (Fig 4B and C). It is possible that some stem cells cannot enter the M phase of the cell cycle after *fbl-2* inhibition, similar to the previous discovery that *fbl* promotes the cell cycle in zebrafish (Bouffard *et al.*, 2018).

Considering the *fbl-2* expression in progenitor cells, we suspected that *fbl-2* was also associated with cell differentiation to maintain tissue homeostasis. Therefore, *fbl-2* KD worms at 7 dpf were chosen to identify the expression levels of progenitors. Notably,

the expression of *prog-1* (an epidermal early progenitor marker) and *hnf4* (an intestinal progenitor and mature cell marker) was disturbed in *fbl-2* KD animals (Fig 4D and E), which further caused abnormalities in epidermal (*AGAT-1*$^+$) and intestine (*gata456*$^+$) morphology. Moreover, the newly differentiated progenitors decreased within the blastema in *fbl-2* KD animals, as indicated by the reduction of *prog-1*$^+$PIWI-1$^+$, *hnf4*$^+$PIWI-1$^+$, and *ovo*$^+$PIWI-1$^+$ cells compared with those in *egfp* KD controls at 24, 48, and 72 hpa (Figs 4F, EV4B). In conclusion, KD of *fbl-2* blocked stem cell proliferation and differentiation during homeostasis and regeneration.

Smed-fbl-1 **is required for epidermal integrity and wound response**

Given the epithelial expression pattern and lesion in tails, we assessed the mature tissue markers to narrow down the specific defects induced by KD of *fbl-1*. The staining of muscle, epidermis, and neurons indicated that *fbl-1* KD destroyed multiple tissue morphologies in homeostasis, which might be explained by a secondary effect of epidermal disruption (Fig 5A). Remarkably, *fbl-1* KD planarians displayed an abnormal pattern of epidermal cells distinct from that of *fbl-2* KD planarians (Fig 5B). Therefore, we chose different time points to examine the dynamic expression of epithelial cells. The distribution of *AGAT-1*$^+$ cells in planarians can be separated approximately into three layers according to the morphology and number along the LM axis. FISH and quantification analysis indicated that the total number of *AGAT-1*$^+$ cells decreased, especially those cells closed to the body boundary (layer 1) at 7 dpf (Fig 5C and D). Until 21 dpf, all the worms exhibited damaged tails or died, the expression of *vim-3* in the wound site was disturbed, and *AGAT-1*$^+$ cells were accumulated (Fig 5E). Consistent with the defects in homeostasis, loss of epithelial integrity and cell numbers also occurred to *fbl-1* KD worms after amputation (Figs 5F and G, EV5G). These results suggested that during homeostasis and regeneration, *fbl-1* is required for the specification of *AGAT-1*$^+$ cells into the mature epidermis (e.g., *vim-3*$^+$ cells).

Amputation triggers wound response and neoblasts proliferation to restore missing tissue (Wenemoser & Reddien, 2010). The increase of *fbl-1*$^+$ cells at wound sites and delayed regeneration after KD of *fbl-1* prompted us to explore the balance between

cell proliferation and cell death during regeneration. There are two mitotic peaks at 6 and 48 hpa, whereas cell death is increased at 4 and 72 hpa. We found that KD of *fbl-1* would cause a significant reduction of $H3P^+$ cells at 48 hpa and increased $TUNEL^+$ signals at 72 hpa (Fig EV5E and F). Combined with the results of the analysis above, this evidence indicated that *fbl-1* is required for wound responses and epidermal integrity.

In summary, we proposed that two genes encoding homologs of FBL are essential for planarian tissue homeostasis and regeneration in distinct manners (Fig 6A and B). The *fbl-1* was expressed in epidermal lineage cells and regulated the specification of *AGAT-1*$^+$ cells. The reduced regenerative ability resulted from the loss of wound response at the early time points and from decreases in protein synthesis to trigger epidermal maturation after KD of *fbl-1*. Unlike *fbl-1*, *fbl-2* helped maintain the proliferation of stem cells and regulate the differentiation of multiple cell-lineage progenitors (Fig 6A). The specific modification of FBL in distinct cell types increased the ribosome heterogeneity to preferentially translate the protein required for particular cell types (Fig 6B).

Discussion

FBL was first identified as a nucleolar protein in 1958 (Crick, 1958). This protein is conserved in organisms ranging from archaea to humans and catalyzes rRNA 2'-O-methylation and pre-rRNA processing via phase separation (Yao *et al.*, 2019). FBL is a useful nucleolar marker to examine the dynamics or morphology of the nucleolus during multiple cellular processes. However, numerous studies have demonstrated its functions in regulating stem cell survival, proliferation, differentiation, and even embryonic development in mice, which explicitly utilize rRNA modification and rRNA transcription (Morral *et al*, 2020; Zhang *et al.*, 2014). Recent studies have proven the existence of ribosome heterogeneity in Drosophila, which can be decided by rRNA variants and RPs (Genuth & Barna, 2018). The KD of *fbl* will reduce the rRNA modification, which can be used as a tool to elucidate how ribosome heterogeneity determines cell fate and nucleolar protein-regulated tissue regeneration (Erales *et al*, 2017; Jansson *et al*, 2021). Therefore, we investigated FBL in distinct planarian cell

types to link its function with cell lineage development underlying ribosome heterogeneity (Fig 6A and B). This provides evidence to understand how epidermal cell differentiation is precisely regulated by the differential expression of *fbl-1* and *fbl-2* in early and late stages, which is divergent from other cell lineages such as intestinal and neural lineages. Further studies on how FBL-mediated modification of rRNA sites and the recognition of mRNA by cell-type-specific ribosomes regulate the “on” and “off” cell fate decisions are needed.

Regeneration requires a precise response to missing tissue. Previous studies on wound response gene expression have revealed that three cell types are activated in response to wounding, including neoblasts, epidermal cells, and muscle cells, in which cell-type-specific genes are expressed (Wurtzel *et al.*, 2015). In parallel with these findings, *fbl-1*$^{+}$ epidermal cells responded to wounds, and the regenerative capacity was impaired after *fbl-1* inhibition. Given the multiple distinct steps of the epidermal lineage development, this discovery may explain how ribosome heterogeneity during regeneration regulates cell-type-specific gene expression in epidermal cells (Pearson & A, 2010; Scimone *et al*, 2010; Tu *et al.*, 2015; van Wolfswinkel *et al*, 2014; Zhu *et al.*, 2015; Zhu & Pearson, 2018). Adopting an additional homolog of FBL provides an advantage in efficiently regulating the sequential requirement of ribosome heterogeneity for further differentiation beyond *AGAT-1*$^{+}$ cells. Although regeneration capacity was diverse among multiple species, the depletion of *fbl* destroyed the transition of stem cells states in mice and zebrafish (Bouffard *et al.*, 2018; Wu *et al*, 2022). All these findings suggested that the ability of FBL to regulate stem cell differentiation in physiological homeostatic and tissue regeneration may be conserved among multiple species.

Materials and methods

Animal maintenance and irradiation

The *Schmidtea mediterranea* CIW4 planarian strain was cultured in 1X Montjuic water at 20°C. The experimental animals were starved for up to 7 days. For irradiation, 4 ~ 5 mm worms were exposed to 60 Gy of radiation by an RS2000 Pro X-ray irradiation

apparatus.

RNA extraction, gene cloning, and expression analysis

Total RNA was extracted with TRIzol (Invitrogen, 10296010) and reverse-transcribed into cDNA with ABScript II-RT Mix for qPCR with gDNA Remover (ABclonal, RK20403) for gene cloning. The primers for gene cloning were designed according to the transcriptome database (https://planosphere.stowers.org/), and the primers for qPCR were designed by an online website (https://simrbase.stowers.org/cgi-bin/primer3.pl), as follows: *fbl-1*: 5' AAGGCCTCTTGTATCGATTC and 3' CCATTGACAGCCAAGATTTC; *fbl-2*: 5' TTTCCAGCATCAGGTGAAAG and 3' ATCTCCAAATCCTCCCCTAC; 18S rRNA: 5' AACGGCTACCACATCC and 3' ACCAGACTTGCCCTCC; and 28S rRNA: 5' CGGATTGTTTGAGAATGCA and 3' CAAAGTTCTTTTCAACTTTCCC. The genes were cloned into the pT4P vector for riboprobes and RNA interference food preparation. Three biological repeats were collected from each group for RNA extraction and gene expression analysis.

Plasmid construction and cell transfection

Each of the full-length FBL homologs in planarians optimized for the human sequence (Genewiz, Inc.) was fused with a 3X Myc tag for transfection to 293T cells, and with 3X Flag tag for transfection to H9 cells. 293T cells were maintained in DMEM (Shanghai Basalmedia Technologies Co., Ltd., L110KJ) with 10% FBS (Excell Bio, FSP500) at 37°C under 5% CO_2. The 293T cells were seeded in a 6-well plate with coverslips and grown to 70% confluence for transfection with Lipofectamine 3000 reagent (Thermo Fisher Scientific, L3000001) as recommended in the kit literature. H9 cells were cultured in mTeSR™ Plus media (STEMCELL, 100-0276) supplemented with 1% Penicillin-Streptomycin (Gibco, 15140122). 400,000 H9 cells for each condition were electroporated with 1 μg plasmid via a human stem cell nucleofector™ kit (VPH-5012) by Lonza AMAXA Nucleofector 2B.

Phylogenetic analysis

The protein sequences of the FBL homologs were downloaded from the websites

https://www.uniprot.org/ and https://planosphere.stowers.org/. The FASTA files of the sequences were generated by MEGA version 6 (Tamura *et al*, 2013). All the protein sequences were aligned online MAFFT version 7 with the L-INS-i method (https://mafft.cbrc.jp/alignment/server/index.html) (Katoh *et al*, 2019; Kuraku *et al*, 2013) and trimmed in MEGA 6. Maximum likelihood analyses were run using the online web server IQ TREE (http://iqtree.cibiv.univie.ac.at/) (Hoang *et al*, 2018; Nguyen *et al*, 2015) with 1,000 ultrafast bootstrap replicates, the WAG amino acid substitution model, four substitution rate categories and the proportion of invariable sites estimated from the dataset. The tree was produced by MEGA 6.

Antibody staining

After 48 h of transfection, cells on coverslips were fixed with 4% paraformaldehyde (PFA) for 45 min and permeabilized with 0.5% PBSTx. The cells were blocked in 5% horse serum for one hour and incubated with anti-MYC primary antibody (SCBT, 9E10) at a 1:500 dilution or anti-FLAG M2 (Sigma, F1804) at a 1:400 dilution overnight at 4°C. The cells were washed with 0.3% PBSTx four times for 15 min per wash and incubated in Alexa Fluor 488 Goat Anti-Mouse IgG H&L (Abcam, ab150117) at a 1:1000 dilution at room temperature (RT) for two hours. The cells were mounted with ProLong™ Gold Antifade Mountant (Thermo Fisher Scientific, P36934) before being stained with DAPI for 15 min at a 1:1000 dilution.

RNAi experiment

pT4P with the genes of interest was transferred into the *E. coli* HT115 strain, and a single colony was cultured for 16 h as a starter culture in 2X YT medium. The starter culture was allowed to grow tenfold before induction with 1 mM IPTG for two hours until the OD600 was approximately 0.8. The 4X RNAi food for *fbl-2* KD was prepared by mixing 50 mL of cultured bacteria with 125 µL of liver homogenate (90% liver paste, 5.5% 1X Montjuic water, and 4.5% red food coloring). The 2X concentration of RNAi food was prepared for *fbl-1* KD. The feeding schedule was arranged according to practical necessity (to produce the desired phenotype but no lethality). The *fbl-1* KD and *fbl-2* KD planarians were fed every three days for a total of five and six times,

respectively, and collected the samples after 7-day starvation.

WISH and FISH

The worms were killed with 5% N-acetylcysteine (NAC) for 5 minutes and fixed with 4% formaldehyde (FA) for 45 minutes following reduction and dehydration. After 2 h of incubation in 100% methanol, the worms were used to perform WISH and FISH experiments. The worms were hybridized with riboprobe in Hybe for up to 16 h at 56°C after being bleached in 5% deionized formamide in 0.5X SSC in direct light for 1.5 h and permeabilized in proteinase K for 10 min. For WISH, the worms were incubated with anti-DIG conjugated with AP overnight at 4°C, and the color was developed with NBT and BCIP. For FISH, the worms were incubated with anti-DIG/DNP/FL conjugated with POD or HRP at 4°C overnight and developed with tyramine labeled with fluorescence at RT for one hour. The anti-H3P and anti-6G10 antibody staining was performed after FISH. The anti-Smed-FBL-2 antibody (antigen aa 2-19, Abclonal Inc.) was used at a 1:500 dilution after worms were bleached and permeabilized. The anti-Smed-PIWI-1 antibody was a gift from J. Rink and was used at a 1:10000 dilution.

Image acquisition and analysis

WISH samples and live worms were imaged on a Leica M205 FA fluorescence stereomicroscope. FISH samples were imaged on a Nikon C2Si inverted confocal microscope. The images were processed in Fiji, Adobe Photoshop, and Adobe Illustrator CC 2018.

Acknowledgments

We thank all the members of the Lei lab and biomedical research core facilities at Westlake University for their technical support. KL was supported by the National Natural Science Foundation of China (31970750, 32122032) and the start-up fund from the Westlake Education Foundation.

Author contributions

Jiajia Chen: Conceptualization; methodology; validation; investigation; data curation; formal analysis; visualization; writing - original draft; writing - review and editing. **Xue**

Pan: Supervision; methodology; validation; investigation. **Hao Xu:** Validation; investigation. **Yuhong Zhang:** Validation; investigation. **Kai Lei:** Conceptualization; methodology; validation; investigation; data curation; formal analysis; visualization; writing - original draft; writing - review and editing.

Conflict of Interest

The authors declare that they have no conflict of interest.

References

Bianco C, Mohr I (2019) Ribosome biogenesis restricts innate immune responses to virus infection and DNA. Elife 8

Bohr TE, Shiroor DA, Adler CE (2021) Planarian stem cells sense the identity of the missing pharynx to launch its targeted regeneration. Elife 10

Boser A, Drexler HC, Reuter H, Schmitz H, Wu G, Scholer HR, Gentile L, Bartscherer K (2013) SILAC proteomics of planarians identifies Ncoa5 as a conserved component of pluripotent stem cells. Cell Rep 5: 1142-1155

Bouffard S, Dambroise E, Brombin A, Lempereur S, Hatin I, Simion M, Corre R, Bourrat F, Joly JS, Jamen F (2018) Fibrillarin is essential for S-phase progression and neuronal differentiation in zebrafish dorsal midbrain and retina. Dev Biol 437: 1-16

Cheng LC, Tu KC, Seidel CW, Robb SMC, Guo F, Sánchez Alvarado A (2018) Cellular, ultrastructural and molecular analyses of epidermal cell development in the planarian Schmidtea mediterranea. Dev Biol 433: 357-373

Crick FH (1958) On protein synthesis. Symp Soc Exp Biol 12: 138-163

Eisenhoffer GT, Kang H, Sánchez Alvarado A (2008) Molecular analysis of stem cells and their descendants during cell turnover and regeneration in the planarian Schmidtea mediterranea. Cell Stem Cell 3: 327-339

Erales J, Marchand V, Panthu B, Gillot S, Belin S, Ghayad SE, Garcia M, Laforets F, Marcel V, Baudin-Baillieu A et al (2017) Evidence for rRNA 2'-O-methylation plasticity: Control of intrinsic translational capabilities of human ribosomes. Proc Natl Acad Sci U S A 114: 12934-12939

Gay DM, Lund AH, Jansson MD (2022) Translational control through ribosome heterogeneity and functional specialization. Trends Biochem Sci 47: 66-81

Genuth NR, Barna M (2018) The Discovery of Ribosome Heterogeneity and Its Implications for Gene Regulation and Organismal Life. Mol Cell 71: 364-374

Hoang DT, Chernomor O, von Haeseler A, Minh BQ, Vinh LS (2018) UFBoot2: Improving the Ultrafast Bootstrap Approximation. Mol Biol Evol 35: 518-522

Jansson MD, Hafner SJ, Altinel K, Tehler D, Krogh N, Jakobsen E, Andersen JV, Andersen KL, Schoof EM, Menard P et al (2021) Regulation of translation by site-specific ribosomal RNA methylation. Nat Struct Mol Biol 28: 889-899

Kang J, Brajanovski N, Chan KT, Xuan J, Pearson RB, Sanij E (2021) Ribosomal proteins and human diseases: molecular mechanisms and targeted therapy. Signal Transduct Target Ther 6: 323

Katoh K, Rozewicki J, Yamada KD (2019) MAFFT online service: multiple sequence alignment, interactive sequence choice and visualization. Brief Bioinform 20: 1160-1166

Krogh N, Jansson MD, Hafner SJ, Tehler D, Birkedal U, Christensen-Dalsgaard M, Lund AH, Nielsen H (2016) Profiling of 2'-O-Me in human rRNA reveals a subset of fractionally modified positions and provides evidence for ribosome heterogeneity. Nucleic Acids Res 44: 7884-7895

Kuraku S, Zmasek CM, Nishimura O, Katoh K (2013) aLeaves facilitates on-demand exploration of metazoan gene family trees on MAFFT sequence alignment server with enhanced interactivity. Nucleic Acids Res 41: W22-28

Lei K, Thi-Kim Vu H, Mohan RD, McKinney SA, Seidel CW, Alexander R, Gotting K, Workman JL, Sánchez Alvarado A (2016) Egf Signaling Directs Neoblast Repopulation by Regulating Asymmetric Cell Division in Planarians. Dev Cell 38: 413-429

Li D, Wang J (2020) Ribosome heterogeneity in stem cells and development. J Cell Biol 219

Li D, Zhang J, Wang M, Li X, Gong H, Tang H, Chen L, Wan L, Liu Q (2018) Activity dependent LoNA regulates translation by coordinating rRNA transcription and methylation. Nat Commun 9: 1726

Lv K, Gong C, Antony C, Han X, Ren JG, Donaghy R, Cheng Y, Pellegrino S, Warren AJ, Paralkar VR et al (2021) HectD1 controls hematopoietic stem cell regeneration by coordinating ribosome assembly and protein synthesis. Cell Stem Cell 28: 1275-1290 e1279

Morral C, Stanisavljevic J, Hernando-Momblona X, Mereu E, Alvarez-Varela A, Cortina C, Stork D, Slebe F, Turon G, Whissell G et al (2020) Zonation of Ribosomal DNA Transcription Defines a Stem Cell Hierarchy in Colorectal Cancer. Cell Stem Cell 26: 845-861 e812

Newton K, Petfalski E, Tollervey D, Caceres JF (2003) Fibrillarin is essential for early development and required for accumulation of an intron-encoded small nucleolar RNA in the mouse. Mol Cell Biol 23: 8519-8527

Nguyen LT, Schmidt HA, von Haeseler A, Minh BQ (2015) IQ-TREE: a fast and effective stochastic algorithm for estimating maximum-likelihood phylogenies. Mol Biol Evol 32: 268-274

Pearson BJ, Sánchez Alvarado A (2010) A planarian p53 homolog regulates proliferation and self-renewal in adult stem cell lineages. Development 137: 213-221

Pelletier J, Thomas G, Volarević S (2018) Ribosome biogenesis in cancer: new players and therapeutic avenues. Nat Rev Cancer 18: 51-63

Pereira-Santana A, Gamboa-Tuz SD, Zhao T, Schranz ME, Vinuesa P, Bayona A, Rodriguez-Zapata LC, Castano E (2020) Fibrillarin evolution through the Tree of Life: Comparative genomics and microsynteny network analyses provide new insights into the evolutionary history of Fibrillarin. PLoS Comput Biol 16: e1008318

Reddien PW (2018) The Cellular and Molecular Basis for Planarian Regeneration. Cell 175: 327-345

Reddien PW (2021) Positional Information and Stem Cells Combine to Result in Planarian Regeneration. Cold Spring Harb Perspect Biol

Reddien PW, Oviedo NJ, Jennings JR, Jenkin JC, Sánchez Alvarado A (2005) SMEDWI-2 is a PIWI-like protein that regulates planarian stem cells. Science 310: 1327-1330

Ren X, Hu B, Song M, Ding Z, Dang Y, Liu Z, Zhang W, Ji Q, Ren R, Ding J et al (2019) Maintenance of Nucleolar Homeostasis by CBX4 Alleviates Senescence and Osteoarthritis. Cell Rep 26: 3643-3656 e3647

Rodriguez-Corona U, Sobol M, Rodriguez-Zapata LC, Hozak P, Castano E (2015) Fibrillarin from Archaea to human. Biol Cell 107: 159-174

Sanchez CG, Teixeira FK, Czech B, Preall JB, Zamparini AL, Seifert JR, Malone CD, Hannon GJ, Lehmann R (2016) Regulation of Ribosome Biogenesis and Protein Synthesis Controls Germline Stem Cell Differentiation. Cell Stem Cell 18: 276-290

Scimone ML, Kravarik KM, Lapan SW, Reddien PW (2014) Neoblast specialization in regeneration of the planarian Schmidtea mediterranea. Stem Cell Reports 3: 339-352

Scimone ML, Meisel J, Reddien PW (2010) The Mi-2-like Smed-CHD4 gene is required for stem cell differentiation in the planarian Schmidtea mediterranea. Development 137: 1231-1241

Tamura K, Stecher G, Peterson D, Filipski A, Kumar S (2013) MEGA6: Molecular Evolutionary Genetics Analysis version 6.0. Mol Biol Evol 30: 2725-2729

Tu KC, Cheng LC, H TKV, Lange JJ, McKinney SA, Seidel CW, Sánchez Alvarado A (2015) Egr-5 is a post-mitotic regulator of planarian epidermal differentiation. Elife 4: e10501

van Wolfswinkel JC, Wagner DE, Reddien PW (2014) Single-cell analysis reveals functionally distinct classes within the planarian stem cell compartment. Cell Stem Cell 15: 326-339

Wagner DE, Ho JJ, Reddien PW (2012) Genetic regulators of a pluripotent adult stem cell system in planarians identified by RNAi and clonal analysis. Cell Stem Cell 10: 299-311

Watanabe-Susaki K, Takada H, Enomoto K, Miwata K, Ishimine H, Intoh A, Ohtaka M, Nakanishi M, Sugino H, Asashima M et al (2014) Biosynthesis of ribosomal RNA in

nucleoli regulates pluripotency and differentiation ability of pluripotent stem cells. Stem Cells 32: 3099-3111

Wenemoser D, Lapan SW, Wilkinson AW, Bell GW, Reddien PW (2012) A molecular wound response program associated with regeneration initiation in planarians. Genes Dev 26: 988-1002

Wenemoser D, Reddien PW (2010) Planarian regeneration involves distinct stem cell responses to wounds and tissue absence. Dev Biol 344: 979-991

Wu Q, Shichino Y, Abe T, Suetsugu T, Omori A, Kiyonari H, Iwasaki S, Matsuzaki F (2022) Selective translation of epigenetic modifiers affects the temporal pattern and differentiation of neural stem cells. Nat Commun 13: 470

Wurtzel O, Cote LE, Poirier A, Satija R, Regev A, Reddien PW (2015) A Generic and Cell-Type-Specific Wound Response Precedes Regeneration in Planarians. Dev Cell 35: 632-645

Xu X, Xiong X, Sun Y (2016) The role of ribosomal proteins in the regulation of cell proliferation, tumorigenesis, and genomic integrity. Sci China Life Sci 59: 656-672

Yao RW, Xu G, Wang Y, Shan L, Luan PF, Wang Y, Wu M, Yang LZ, Xing YH, Yang L et al (2019) Nascent Pre-rRNA Sorting via Phase Separation Drives the Assembly of Dense Fibrillar Components in the Human Nucleolus. Mol Cell 76: 767-783 e711

Yi Y, Li Y, Meng Q, Li Q, Li F, Lu B, Shen J, Fazli L, Zhao D, Li C et al (2021) A PRC2-independent function for EZH2 in regulating rRNA 2'-O methylation and IRES-dependent translation. Nat Cell Biol 23: 341-354

Zhang Q, Shalaby NA, Buszczak M (2014) Changes in rRNA transcription influence proliferation and cell fate within a stem cell lineage. Science 343: 298-301

Zhu SJ, Hallows SE, Currie KW, Xu C, Pearson BJ (2015) A mex3 homolog is required for differentiation during planarian stem cell lineage development. Elife 4

Zhu SJ, Pearson BJ (2018) Smed-myb-1 Specifies Early Temporal Identity during Planarian Epidermal Differentiation. Cell Rep 25: 38-46 e33

Figure legends

Figure 1 Chen et al.

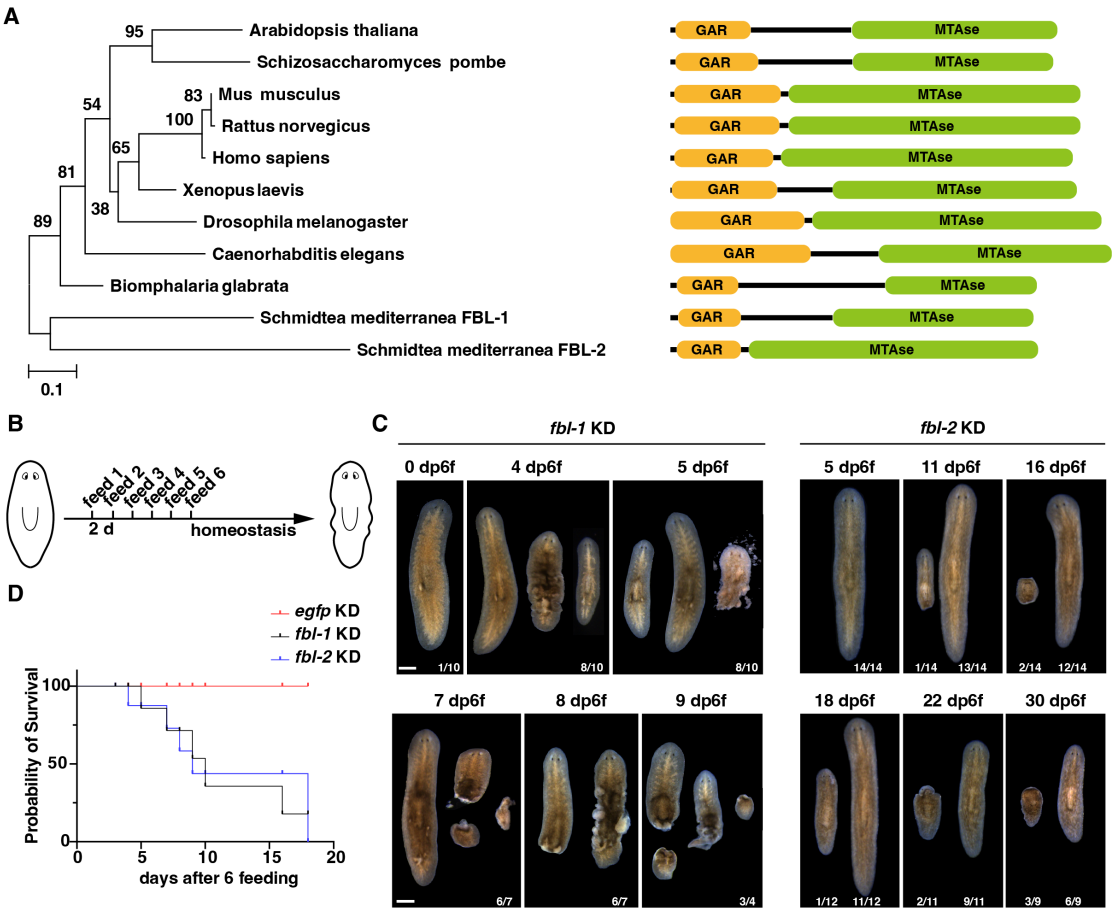

Figure 1. *fbl-1* and *fbl-2* are required for tissue homeostasis.

A. Phylogenetic tree of FBL protein homologs from 10 species with a schematic diagram of the functional domains. The posterior probability value is shown on each branch.

B. Feeding schedule (six times every three days) to examine the function of *fbl-1* and *fbl-2* in homeostasis.

C. Different effects on homeostasis caused by KD of *fbl-1* or *fbl-2*. White spots on the dorsal surface and regressing heads of *fbl-2* KD worms in a small population during homeostasis were observed. The number indicates the penetration of defective phenotypes in representative images. Scale bars, 500 μm.

D. Survival curves of animals after KD of *fbl-1* or *fbl-2*.

Figure EV1 Chen et al.

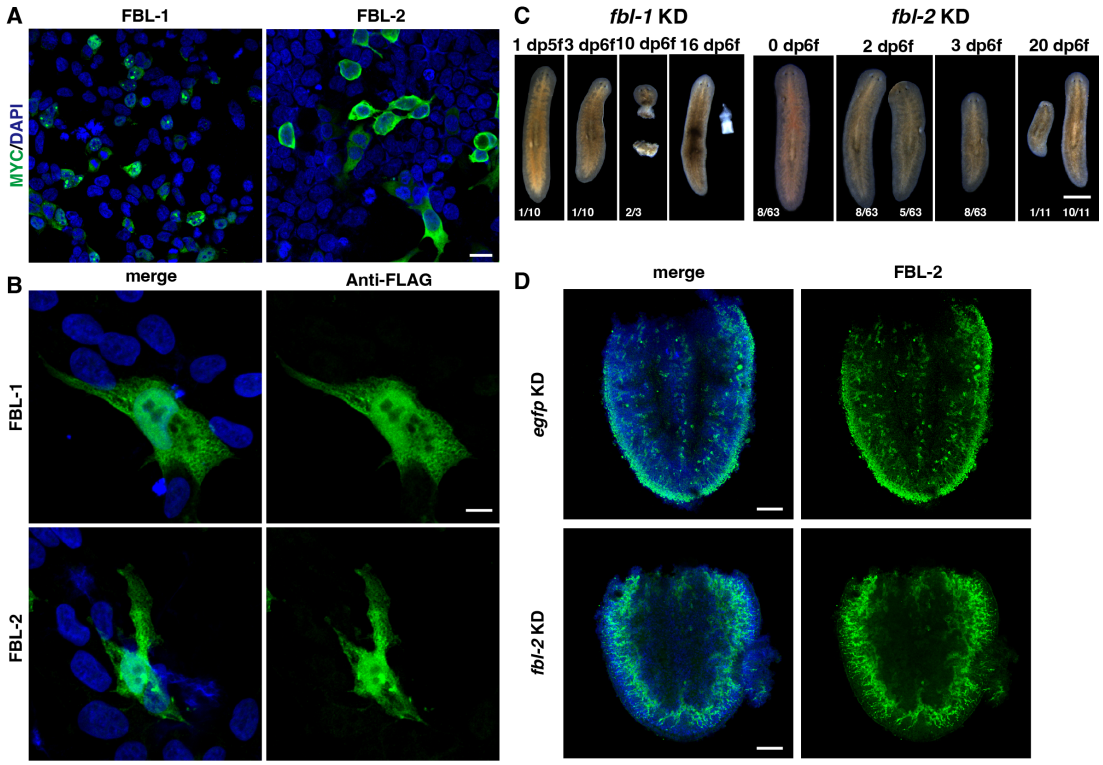

Figure EV1. *fbl-1* and *fbl-2* are required for tissue homeostasis.

A. Expression analysis of FBL-1 and FBL-2 in 293T cells. Scale bar, 20 μm.

B. Expression analysis of FBL-1 and FBL-2 in human embryonic cells H9. Scale bar, 10 μm.

C. Animal phenotype observation after KD of *fbl-1* or *fbl-2*. Scale bar, 500 μm.

D. Reduced expression level of FBL-2 after *fbl-2* KD at 24 hpa. Scale bars, 100 μm.

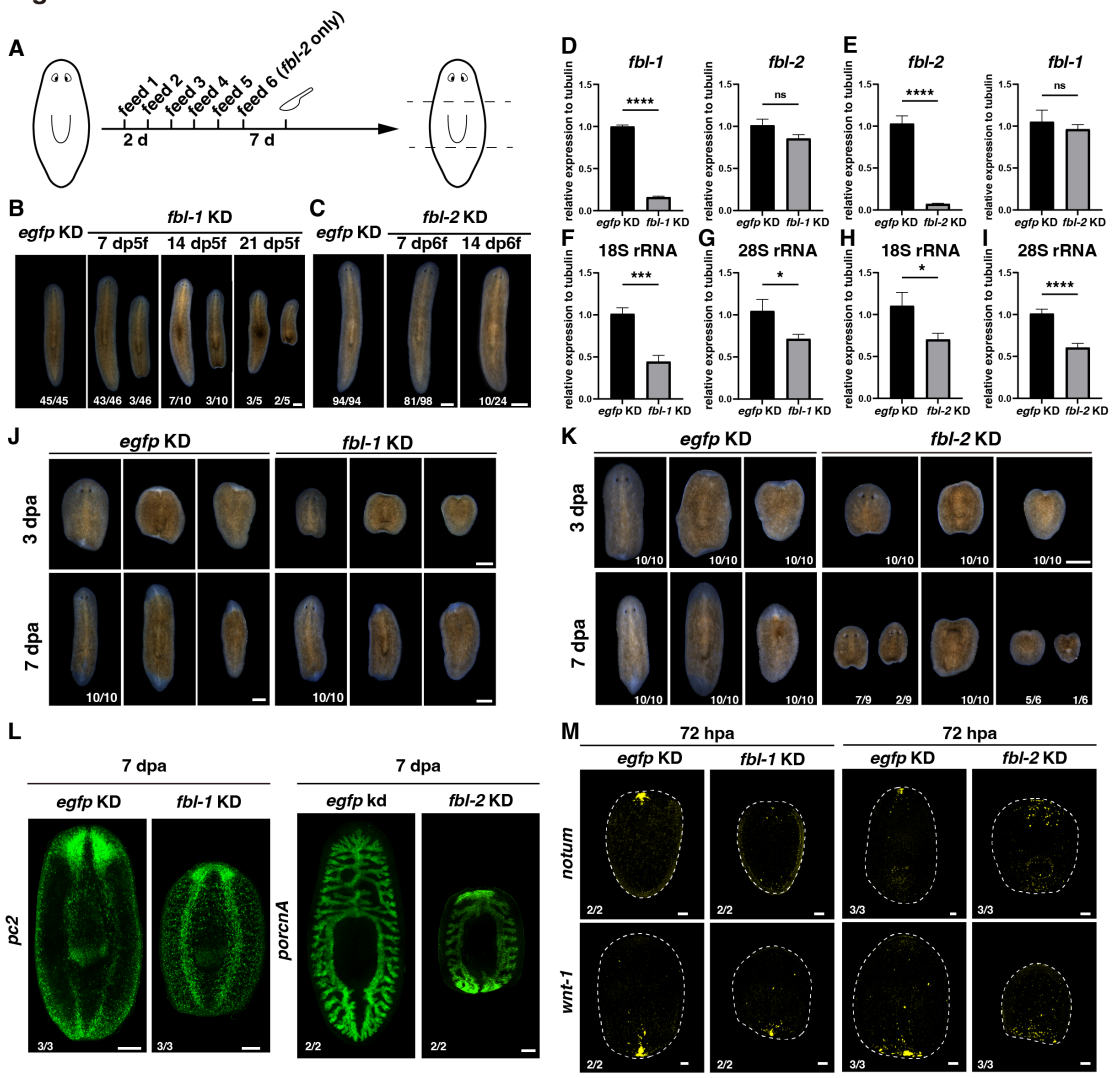

Figure 2. *fbl-1* and *fbl-2* are required for tissue homeostasis and regeneration.

A. Schedule of RNAi feeding every three days and amputation of *fbl-1* and *fbl-2* KD animals.

B, C. Different effects of *fbl-1* KD (B) and *fbl-2* KD (C) on homeostasis under a modified feeding schedule. Scale bars, 500 μm.

D. Relative mRNA level of *fbl-1* and *fbl-2* in *fbl-1* KD animals measured by qPCR.

E. Relative mRNA level of *fbl-1* and *fbl-2* in *fbl-2* KD animals measured by qPCR.

F, G. Relative expression levels of 18S rRNA and 28S rRNA after *fbl-1* KD.

H, I. Relative expression levels of 18S rRNA and 28S rRNA after *fbl-2* KD. ns, not significant; **P* < 0.05; ****P* < 0.001; *****P* < 0.0001 (Student's *t*-test).

J. *fbl-1* KD causes regenerative delay. Scale bars, 500 μm.

K. Regenerative defects of *fbl-2* KD animals at 3 and 7 dpa. Scale bar, 500 μm.

L. Regeneration effects are shown by mature tissue marker expression at 7 dpa (neurons, *pc2*; gut, *porcn A*). Scale bars, 200 μm.

M. Abnormal expression of anterior and posterior pole markers (*notum*, *wnt-1*) at 72 hpa. Scale bars, 100 μm.

Figure EV2 Chen et al.

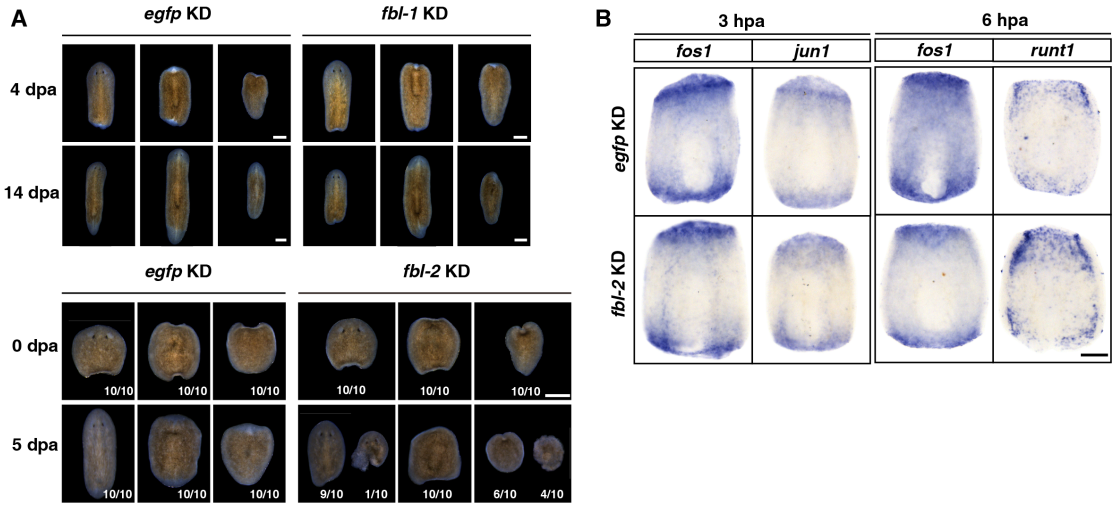

Figure EV2. *fbl-1* and *fbl-2* are required for regeneration.

A. Defects in regeneration after KD of *fbl-1* at 4, 14 dpa, and KD of *fbl-2* at 0, 5 dpa. Scale bars, 500 μm.

B. WISH of wound-induced gene expression levels at 3 and 6 hpa (*jun-1*, *fos-1*, *runt1*) in *fbl-2* KD and *egfp* KD animals. Scale bar, 200 μm.

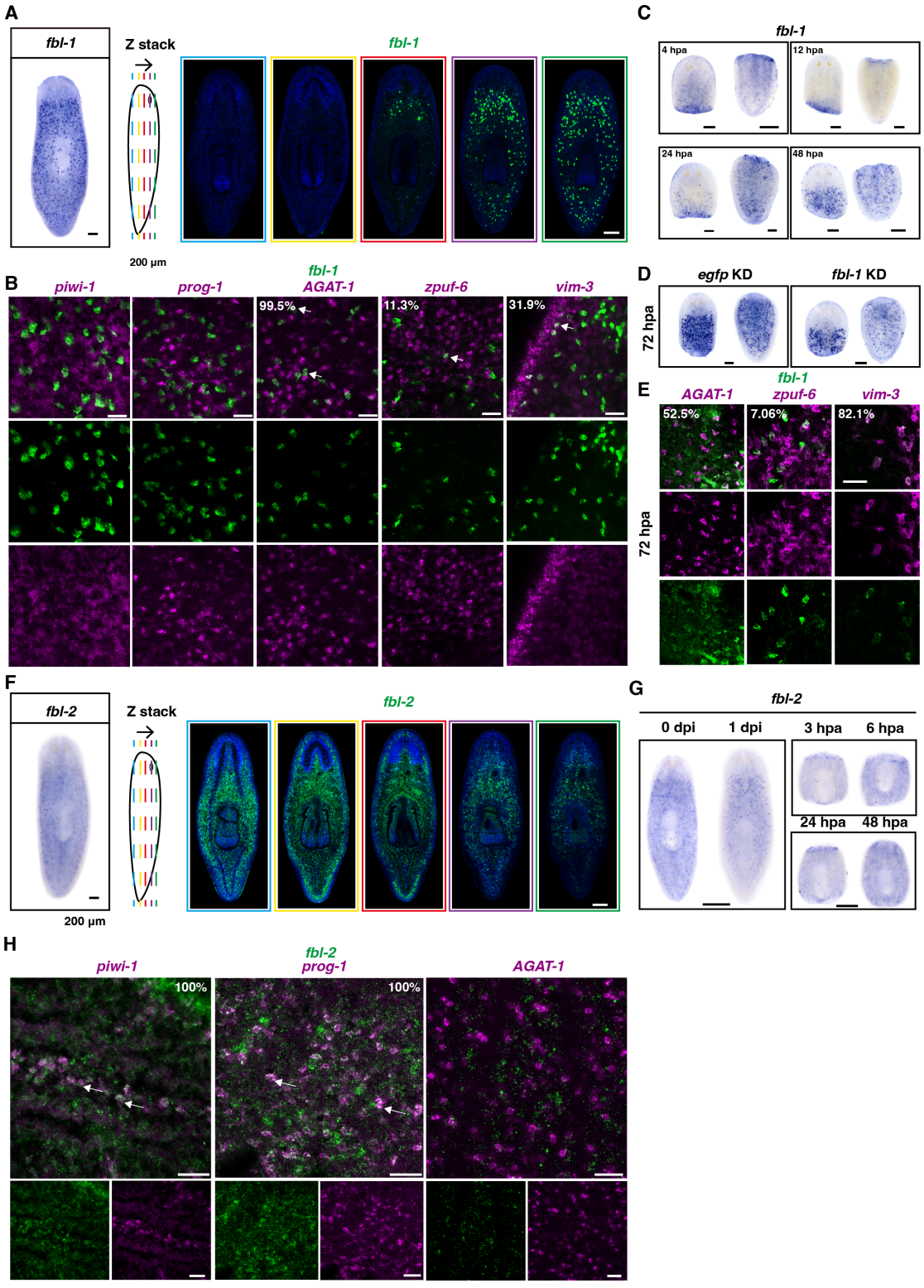

Figure 3. Expression analysis of *fbl-1* and *fbl-2* in distinct cell lineages.

A. The expressed pattern of *fbl-1* in planarians by FISH and *fbl-1* expression pattern is shown as the z stack in planarians. Scale bars, 200 μm.

B. Colocalization of *fbl-1* with epithelial lineage markers (*prog-1*, *AGAT-1*, *zpuf-6*, and

vim-3) in intact worms. The percentages of marker positive cells to *fbl-1* positive cells are shown. Scale bars, 500 μm.

C. *fbl-1* expression responds to injury at the wound site from 4 hpa to 24 hpa. Scale bars, 200 μm.

D. No distinct decrease in *fbl-1* expression was observed at 72 hpa compared with the expression in the control group. Scale bars, 500 μm.

E. Colocalization of *fbl-1* with epithelial lineage markers (*AGAT-1*, *zpuf-6*, and *vim-3*) at 72 hpa. The percentages of marker positive cells to *fbl-1*$^{+}$ cells are shown. Scale bars, 100 μm.

F. The expression pattern of *fbl-2* in planarians as determined by WISH and the *fbl-2* expression pattern shown as a z stack. Scale bars, 200 μm.

G. *fbl-2* expression levels at 0 and 1 dpi and at 3, 6, 24, and 48 hpa. Scale bars, 500 μm.

H. Colocalization of *fbl-2* with a stem cell marker (*piwi-1*), epithelial progenitor marker (*prog-1*), and mature epithelial cell marker (*AGAT-1*). The percentages of *fbl-2* positive cells with indicated cell type markers are shown. White arrow: double-positive cells. Scale bars, 50 μm.

Figure EV3 Chen et al.

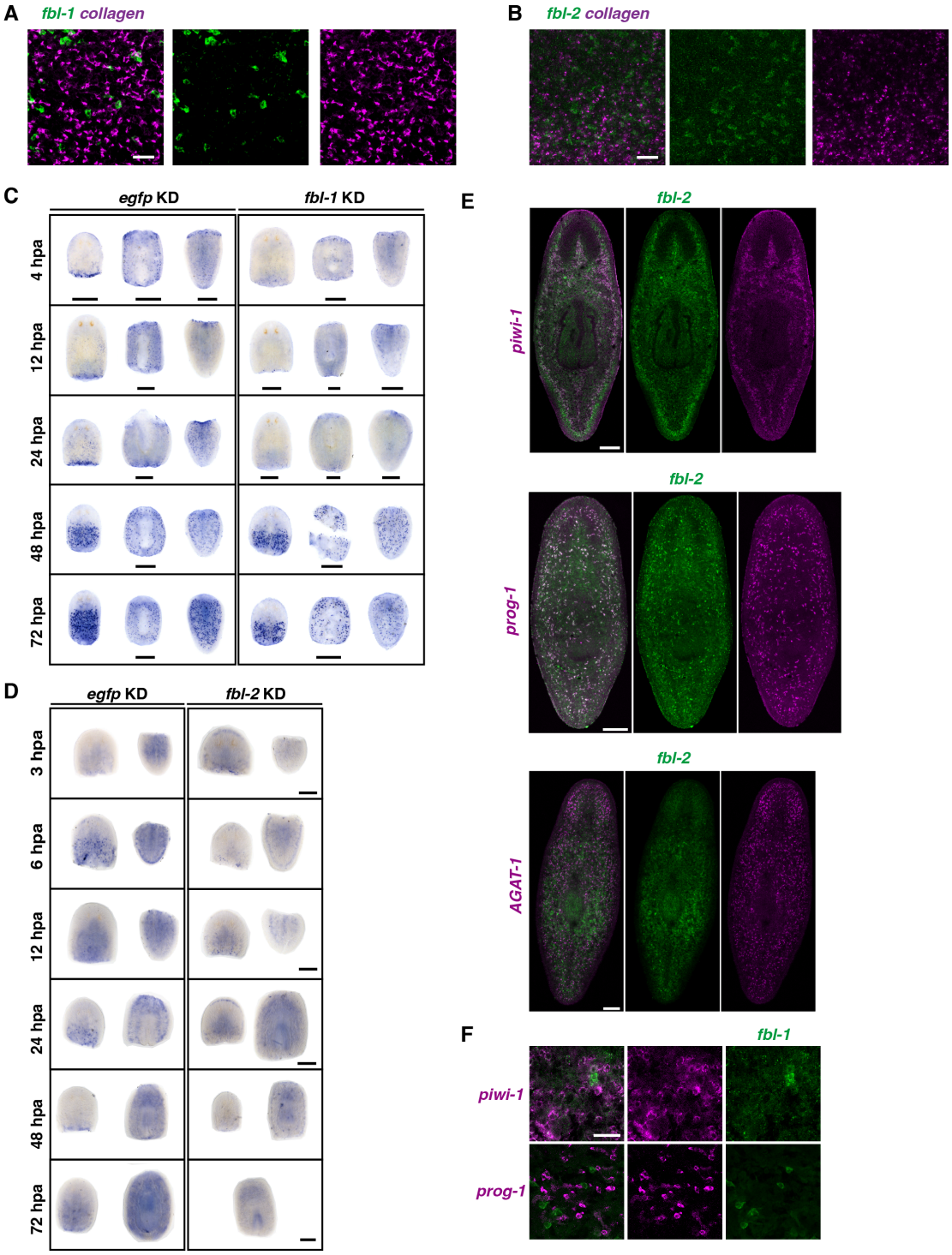

Figure EV3. Expression of *fbl-1* and *fbl-2* in distinct cell lineages.

A, B. No colocalization of the expression of *fbl-1* and *fbl-2* with collagen. Scale bars, 50 μm.

C. *fbl-1* expression at 4, 12, 24, 48, and 72 hpa between the *egfp* KD and *fbl-1* KD groups. Scale bars, 500 μm.

D. *fbl-2* expression at 3, 6, 12, 24, 48, and 72 hpa between the *egfp* KD and *fbl-2* KD groups. Scale bars, 500 μm.

E. *fbl-2* expression with *piwi-1*, *prog-1*, and *AGAT-1* in intact animals. Scale bars, 200 μm.

F. No colocalization of the expression of *fbl-1* with *piwi-1* and *prog-1* at 72 hpa. Scale bar, 100 μm.

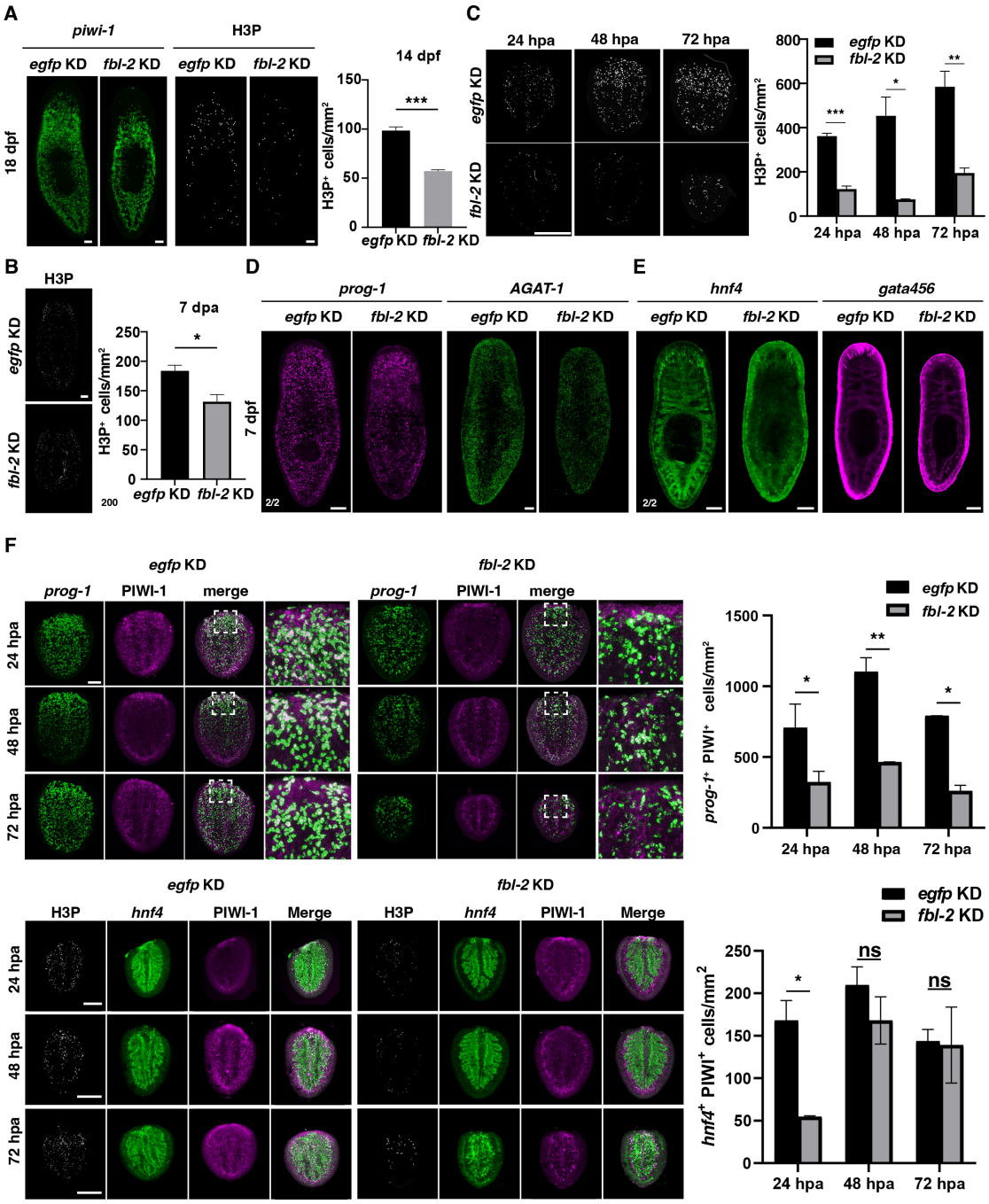

Figure 4. Reduction in cell proliferation and disruption of multiple cell lineage differentiation after *fbl-2* KD.

A. There was no significant difference in stem cells during homeostasis, but a decreased number of proliferated cells, as shown by H3P signals. Scale bars, 100 μm. ***$P < 0.001$ (Student's *t*-test).

B. Cell proliferation and quantification of H3P during regeneration. Scale bar, 200 μm. *$P < 0.05$ (Student's *t*-test).

C. Cell proliferation and quantification of $H3P^{+}$ cells after *fbl-2* KD during regeneration. Scale bar, 500 μm.

D. FISH images show the expression levels of the epidermal progenitor marker *prog-1* and the maturity marker *AGAT-1* during homeostasis in *egfp* KD and *fbl-2* KD animals at 7 dpf. Scale bars, 200 μm.

E. FISH images show the expression levels of the intestinal progenitor marker *hnf4* and the maturity marker *gata456* during homeostasis in *egfp* KD and *fbl-2* KD animals at 7 dpf. Scale bar, 200 μm.

F. *fbl-2* KD blocks progeny (*prog-1*$^{+}$, *hnf4*$^{+}$) differentiation at 24, 48, and 72 hpa, as shown by FISH and quantitation of double positive cells with PIWI-1. Scale bars, 200 μm. **P* < 0.05; ***P* < 0.01 (Student's *t*-test).

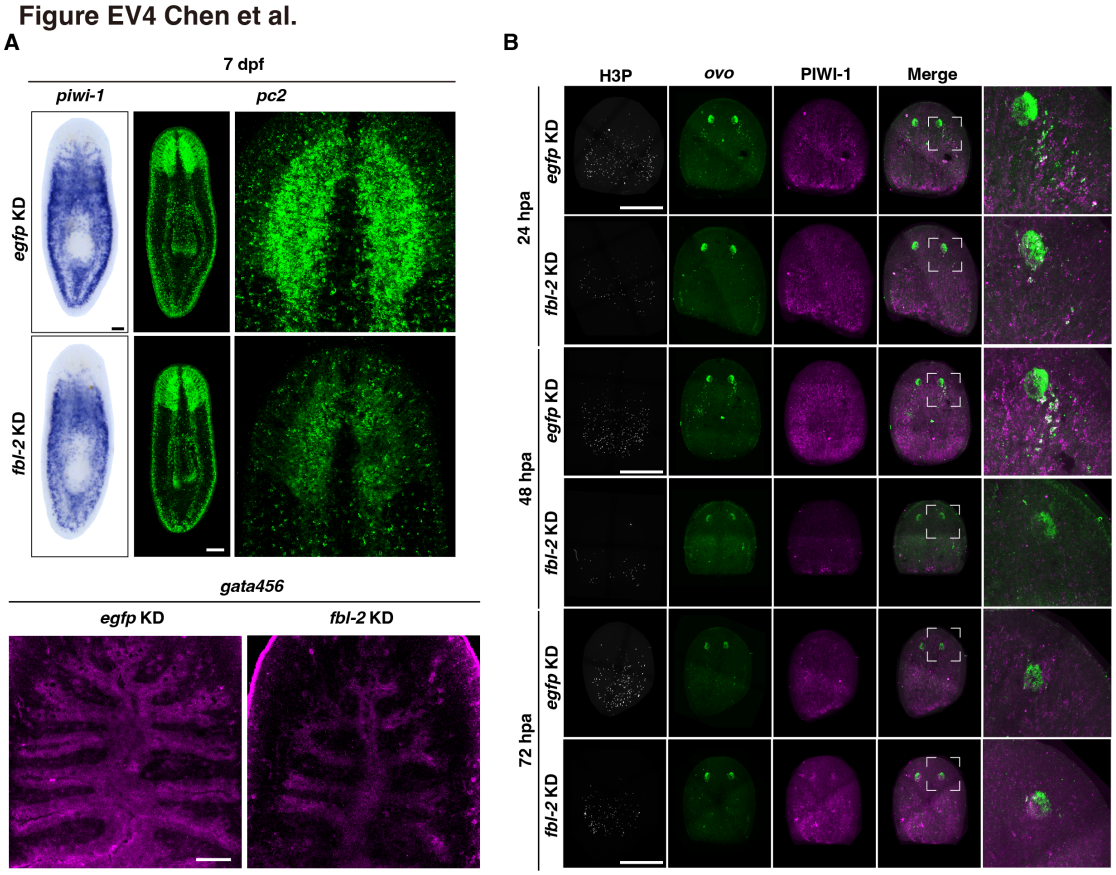

Figure EV4. *fbl-2* is a general master regulator of cell differentiation.

A. Shrinking body size with a slight decrease in the number of stem cells (*piwi-1*) and defects in multiple tissues (neuron, *pc2*; intestine, *gata456*). Scale bars, 100 μm.

B. *fbl-2* KD blocks *ovo*$^{+}$ cell differentiation at 24, 48, and 72 hpa. Scale bars, 200 μm.

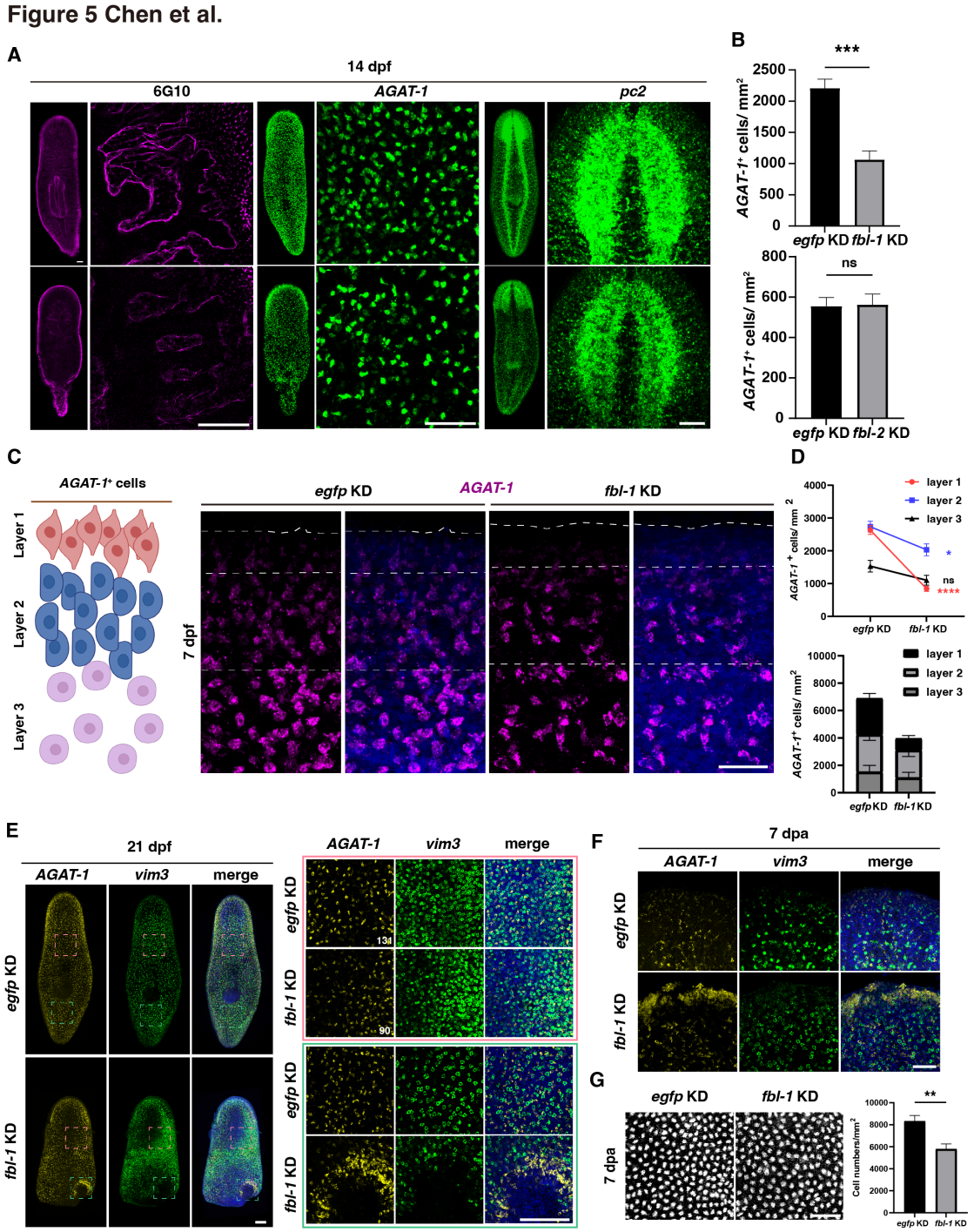

Figure 5. *fbl-1* facilitates the epidermal specification and serves as a wound-induced gene to affect proliferation and cell death during regeneration.

A. *fbl-1* KD causes the loss of muscle, epithelial, and neuronal tissue during homeostasis. Scale bars, 100 μm.

B. Quantification of *AGAT-1*$^+$ cells in *fbl-1* KD and *fbl-2* KD animals at 14 dpf. ***$P <$ 0.001 (Student's *t*-test).

C. Disturbed *AGAT-1*$^+$ cells from FISH-labeled *AGAT-1*$^+$ cells far from the boundary of

the body wall after *fbl-1* KD. Scale bar, 50 μm.

D. Quantification of *AGAT-1*$^{+}$ cells in three layers of the animal body between the *fbl-1* and *egfp* KD groups at 7 dpf. ns, not significant; **P* < 0.05; *****P* < 0.0001 (Student's *t*-test).

E. Loss of cells positive for the epidermal lineage marker *vim-3* in broken tails during homeostasis 21 dpf. Scale bars, 200 μm.

F. *AGAT-1*$^{+}$ cells are stimulated at the wound site at 7 dpa after *fbl-1* KD. Scale bar, 100 μm.

G. DAPI staining and quantification show decreased epidermal cell number after *fbl-1* KD at 7 dpa. Scale bar, 50 μm.

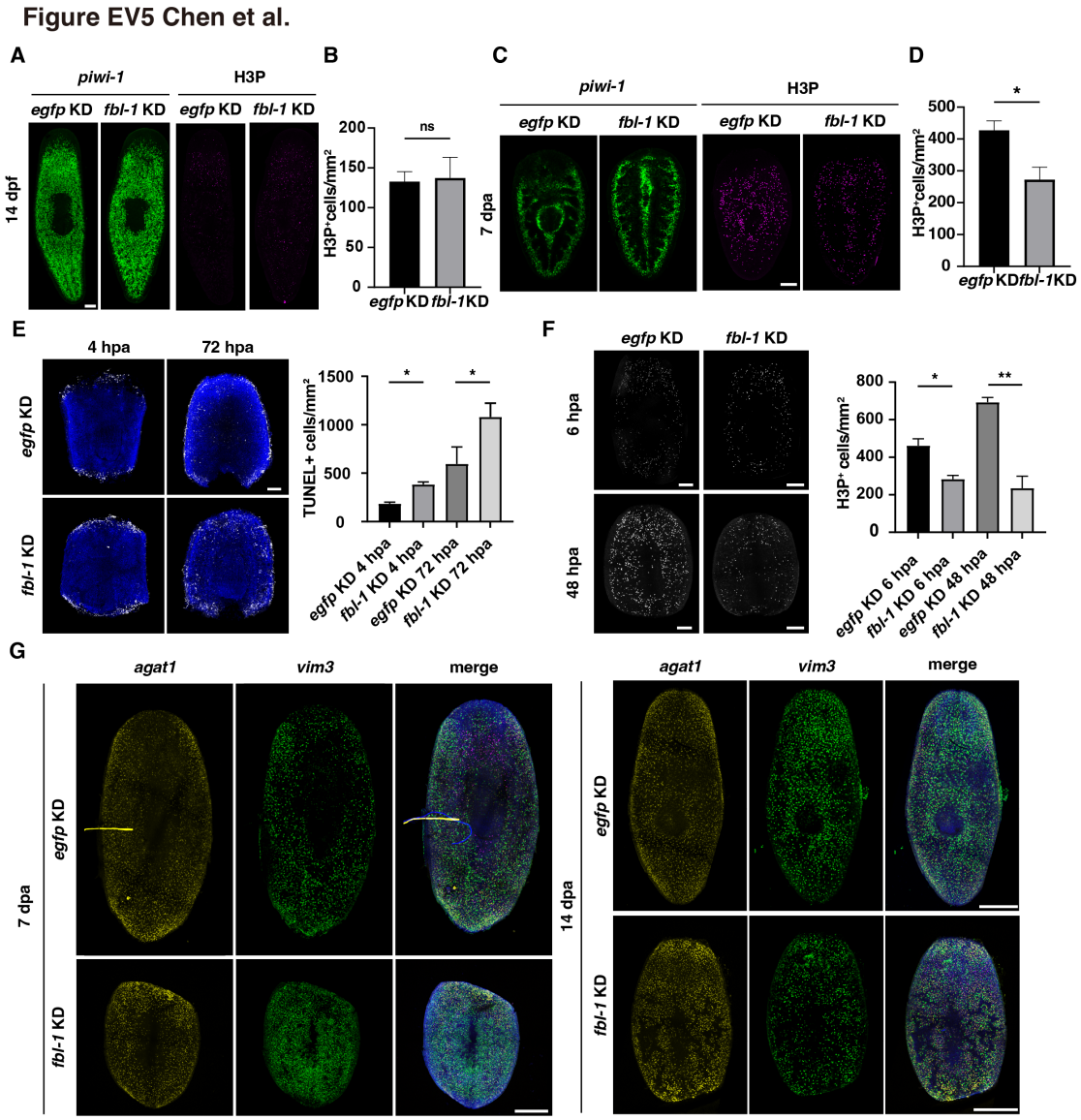

Figure EV5. *fbl-1* inhibition causes secondary defects in stem cell behaviors.

A. No significant changes in stem cell numbers or proliferative cells during homeostasis after *fbl-1* KD. Scale bar, 200 μm.

B. Quantification of $H3P^+$ cells at 14 dpf after *fbl-1* KD.

C. Cell proliferation decreased, but stem cell differentiation increased during regeneration in *fbl-1* KD. Scale bar, 200 μm.

D. Quantification of $H3P^+$ cells at 7 dpa after *fbl-1* KD compared with those in *egfp* KD animals. $*P < 0.05$ (Student's *t*-test).

E. TUNEL staining shows Increased cell death in *fbl-1* KD animals at 4 hpa and 72 hpa. Scale bar, 200 μm.

F. Reduced cell proliferation was revealed by fluorescence staining and quantification

of the $H3P^+$ cells in *fbl-1* KD animals at 6 hpa and 48 hpa. Scale bar, 200 μm. **P* < 0.05; ***P* < 0.01 (Student's *t*-test).

G. Expression of *AGAT-1*$^+$ and *vim3*$^+$ cells during regeneration at 7 dpa and 14 dpa in *egfp* KD and *fbl-1* KD animals. Scale bars, 500 μm.

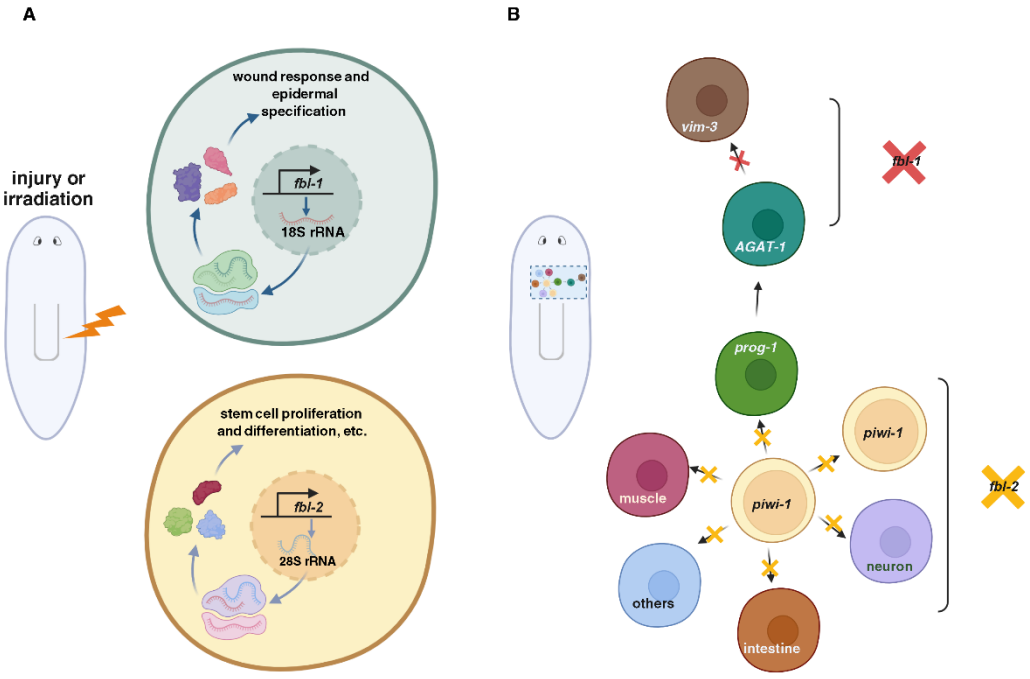

Figure 6. Working model suggests the existence of ribosome heterogeneity regulating cell regeneration during homeostasis and in the context of missing tissue regeneration.

A. *fbl-1* and *fbl-2* regulate planarian homeostasis and regeneration via ribosome heterogeneity.

B. *fbl-1* and *fbl-2* inhibition block the cell fate transition.